JACS JOURNAL OF THE AMERICAN CHEMICAL SOCIETY

Article

Cite This: J. Am. Chem. Soc. 2019, 141, 15942−15950

pubs.acs.org/JACS

Electrocatalytic Hydrogen Evolution from a Cobaloxime-Based Metal−Organic Framework Thin Film

Souvik Roy,[†,§] Zhehao Huang,[‡,§] Asamanjoy Bhunia,[†] Ashleigh Castner,[†] Arvind K. Gupta,[†] Xiaodong Zou,[‡] and Sascha Ott*[,†]

[†]Department of Chemistry − Ångström Laboratory, Uppsala University, Box 523, 751 20 Uppsala, Sweden

[‡]Berzelii Centre EXSELENT on Porous Materials, Department of Materials and Environmental Chemistry, Stockholm University, 106 91 Stockholm, Sweden

Supporting Information

ABSTRACT: Molecular hydrogen evolution catalysts (HECs) are synthetically tunable and often exhibit high activity, but they are also hampered by stability concerns and practical limitations associated with their use in the homogeneous phase. Their incorporation as integral linker units in metal−organic frameworks (MOFs) can remedy these shortcomings. Moreover, the extended three-dimensional structure of MOFs gives rise to high catalyst loadings per geometric surface area. Herein, we report a new MOF that exclusively consists of cobaloximes, a widely studied HEC, that act as metallo-linkers between hexanuclear zirconium clusters. When grown on conducting substrates and under applied reductive potential, the cobaloxime linkers promote electron transport through the film as well as function as molecular HECs. The obtained turnover numbers are orders of magnitude higher than those of any other comparable cobaloxime system, and the molecular integrity of the cobaloxime catalysts is maintained for at least 18 h of electrocatalysis. Being one of the very few hydrogen evolving electrocatalytic MOFs based on a redox-active metallo-linker, this work explores uncharted terrain for greater catalyst diversity and charge transport pathways.

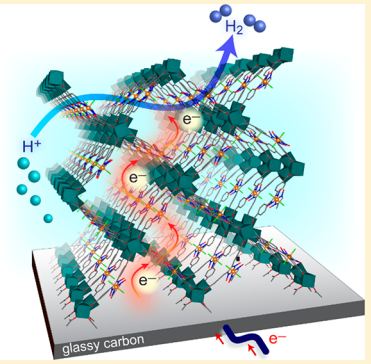

INTRODUCTION

Molecular hydrogen is the ultimate clean fuel due to its extremely high energy density (~142 MJ kg^{-1}) and the fact that its combustion produces only water as "waste" product. However, most hydrogen is currently produced from fossil fuels via steam-methane reforming or gasification of coal.[1−3] Electrochemical water splitting to produce hydrogen from renewable electricity represents a viable option for moving toward a carbon-free energy economy and mitigating the environmental effects associated with greenhouse gas emission.[4−6] Suitable electrocatalysts are required for low kinetic barriers and to drive the reaction at high current densities. *State-of-the-art* solid-state electrocatalysts generally contain precious and expensive metals, most often platinum,[4,7−9] that make their wide scale implementation unfeasible. While earth abundant element based, and often nanostructured, systems[10−13] have been developed as heterogeneous alternatives, molecular catalysts[14] are somewhat hindered by practical issues, mostly associated with poor water solubility and structural instability. On the other hand, molecular catalysts are motivated by the high activity per metal center, as well as the option to design tailor-made ligand structures that allow intricate tuning of the catalysts' redox potentials and catalytic properties. Molecule-derived hybrid solid catalysts have the potential to overcome the shortcomings of molecular catalysis while maintaining their beneficial aspects. Thus, the fabrication of such hybrid electrodes that are chemically robust and combine large surface areas with high catalyst loadings remains a key target.

Metal−organic frameworks (MOFs) are promising materials for catalytic application due to their porosity and modular nature.[15,16] A three-dimensional array of metal complexes (catalysts) linked to inorganic nodes in a MOF that is grown directly on a planar electrode could substantially boost the areal loading of the molecular catalyst, leading to large current densities. In contrast to a densely packed polymerized film, a MOF thin film features a structurally ordered porous network which facilitates diffusion of electrolyte and substrate molecules into the MOF to access also interior catalytic sites. However, the implementation of MOFs as electrocatalysts is limited by their insulating nature and poor charge transport properties.[17−20] This deficiency can be addressed either by orbital overlap and charge delocalization between linkers[21,22] or by introducing redox-active molecular linkers that render the MOFs electroactive by acting as conduits for electron transfer via a hopping mechanism.[23−29] This process is expedited by the proximity of the redox-active linkers in the MOF architecture which, under ideal circumstances, can engage all linkers to mediate charge transport.

Application of this strategy has so far been mostly limited to porphyrin-based three-dimensional (3D) MOFs that have

Received: July 11, 2019
Published: September 11, 2019

DOI: 10.1021/jacs.9b07084
J. Am. Chem. Soc. 2019, 141, 15942−15950

been successfully utilized for electrocatalytic CO_2 reduction reaction (CO_2RR),[30−33] oxygen reduction reaction (ORR),[34] nitrite oxidation,[35] and, very recently, hydrogen evolution[36] where the linkers serve dual roles as charge transport mediators and catalysts. Other reported examples of hydrogen evolving electrocatalysts based on coordination polymers describe either 2D MOFs and metal−organic surfaces (MOSs) with metal-dithiolene/dithiolene-diamine linkers[37−40] or MOFs loaded with amorphous heterogeneous electrocatalysts with the MOF only serving as a porous and electrochemically silent scaffold.[41,42] Designing a three-dimensional architecture composed entirely of hydrogen evolution catalysts (HECs) as metallo-linkers has remained a challenge in the field.

Herein, we report a new 3D MOF that consists exclusively of cobaloxime HEC linkers coordinated to inorganic nodes of zirconium-oxo clusters. The structure of the new MOF, UU-100(Co) (UU = Uppsala University), is determined by microcrystal electron diffraction, known as MicroED,[24,43] or more precisely continuous rotation electron diffraction (cRED) method.[44] Spectroelectrochemical studies on UU-100 grown as thin films on FTO (fluorine doped tin oxide) electrodes allow the quantification of electrochemically accessible cobaloxime units (~57%). When grown on glassy carbon, UU-100(Co) acts as an electrochemical HEC over 18 h with a constant current density of 1.7 mA cm^{-2}. Postelectrolysis studies show that the molecular integrity of the cobaloxime linkers remains intact.

RESULTS AND DISCUSSION

Synthesis and Characterization. Cobaloximes are among the most widely studied molecular HECs[45] and were employed here as metallo-linkers for MOF fabrication. They are known for their high catalytic activity, but their use in homogeneous phase is limited by low structural stability that is caused by the fragile ligand framework around the Co center where the individual oximes are only held together by weak hydrogen bonding. We hypothesized that this design weakness can be overcome by incorporation of the catalyst into a MOF. For this purpose, a tetranucleating cobaloxime linker with carboxylate anchors, $[Co(dcpgH)(dcpgH_2)]Cl_2$ (Figure 1A), was synthesized by metalation of the dioxime, 4,4′-(1,2-bis(hydroxyimino)ethane-1,2-diyl)dibenzoic acid, under aerobic conditions. The solid-state molecular structure of the cobaloxime was determined by X-ray crystallography (Figure S1, Table S1) which shows the expected octahedral geometry around the six-coordinate Co^{III} center with the two dioxime ligands occupying the equatorial plane and the two chloride ligands in the axial positions. The phenyl rings that bear the carboxyl groups are twisted out of the CoN_4 plane due to steric factors with dihedral angles of 47.9° and 42.7° for the two sets of phenyl rings (Figure S2).

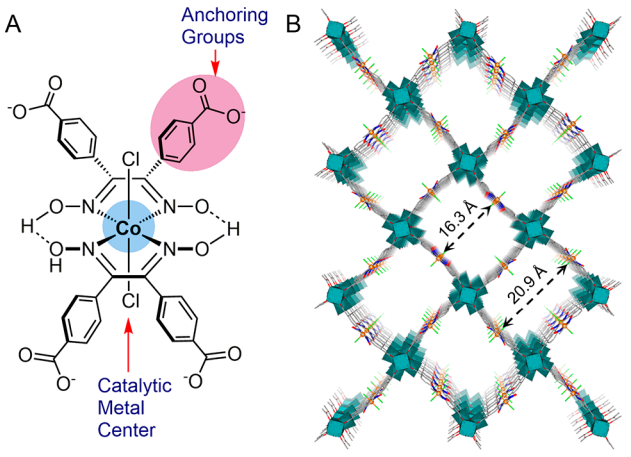

Figure 1. (A) Structure of the cobaloxime linker in UU-100(Co) and (B) structural model of UU-100(Co) MOF viewed along [001].

Crystalline MOF material was synthesized by a "controlled secondary building unit (SBU)" approach that involves preassembly of the zirconium-oxo cluster by reacting $ZrCl_4$ with acetic acid at elevated temperature.[46,47] Subsequent addition of the cobaloxime linker leads to an exchange of the SBU-coordinated acetates by the tetracarboxylate ligands and the formation of the 3D framework. Crystallinity of the resulting MOF, UU-100(Co), was confirmed by powder X-ray diffraction (PXRD), which shows intense peaks in the low angle range, characteristic of porous materials (Figure 2A). The morphology of the MOF particles was examined by scanning electron microscopy (SEM), which shows that the material consists of rod-shaped crystallites ~1−3 μm in length (Figure 2B). Energy dispersive X-ray (EDX) elemental mapping of UU-100(Co) shows uniform distribution of cobalt and zirconium throughout the material (Figures 2B and S8) with an average Zr:Co ratio of 2.4 ± 0.3 (Table S2, Figure S9). The metal content of the MOF was further quantified by ion-coupled plasma optical emission spectroscopy (ICP-OES) which gave a Zr:Co ratio of 2.8 ± 0.3.

The structural constitution of the framework was analyzed by transmission electron microscopy (TEM). A continuous rotation electron diffraction (cRED) method[44] revealed a tetragonal unit cell ($a = b = 27.3$ Å, and $c = 19.6$ Å) with $P4/mbm$ as the likely space group (Figure S10, see the Supporting Information for more details). The unit cell dimensions were further refined by Pawley fitting of the PXRD data ($a = b =$ 28.05(5) Å, and $c = 19.07(3)$Å) (Figures 2A and S11, Table S3). The position of the zirconium clusters within the unit cell was determined from the cRED data by applying the Patterson method. Based on the unit cell, space group, and positions of the zirconium clusters, a structural model of UU-100(Co) was generated using the molecular cobaloxime as linkers and hexanuclear Zr_6 clusters as SBUs and optimized by density functional theory (DFT). The resulting structure has a molecular formula $[Zr_6(\mu_3\text{-}O)_8(OH)_8(\text{cobaloxime})_2]$, with 8 of the 12 octahedral edges of the nodal cluster connected to cobaloxime linkers (Figure 1). The calculated Zr:Co ratio of 3:1 is roughly consistent with ICP-OES and SEM-EDX analysis of UU-100(Co), although slightly lower experimental Zr:Co ratios may suggest missing linker or cluster disorder in the MOF. The ATR-IR spectrum of the MOF contains Zr-μ_3-O stretches at 659 cm^{-1} that originate from the Zr_6 nodes (Figure S12), in line with the proposed model. The modeled structure of UU-100(Co) reveals rectangular channels with elliptical pores caused by the slightly bent structure of the cobaloxime linkers. The distances between two cobalt centers across the channel are 16.3 and 20.9 Å, yielding accessible pores with 9.0 Å in width and 13.1 Å in length. High resolution transmission electron microscopy (HRTEM) images along [110] (Figure 2C−E) of UU-100(Co) display clearly lattice fringes which correspond to the (001) planes (d_{001} = 19.1 Å) of the structural model. The cobaloxime linker in UU-100(Co) is structurally similar to the pyrene-based linker of NU-901, and the two MOFs thus display certain structural similarities.[27]

DOI: 10.1021/jacs.9b07084
J. Am. Chem. Soc. 2019, 141, 15942−15950

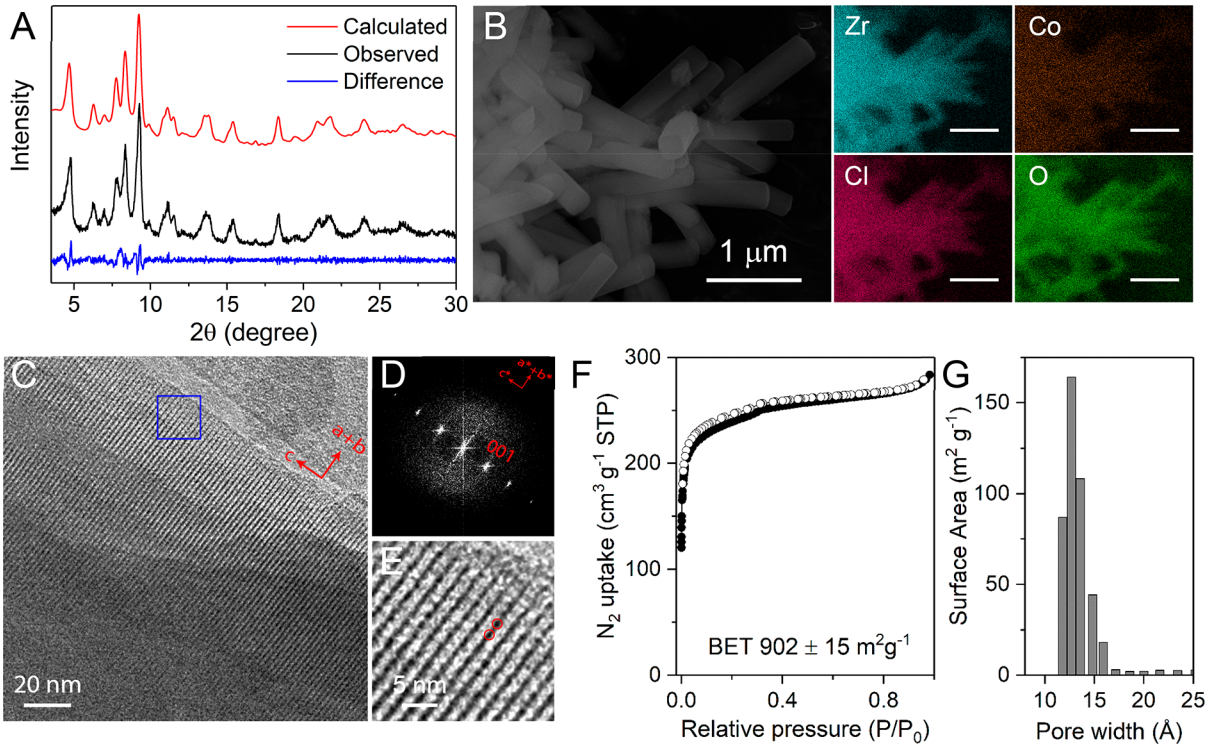

Figure 2. (A) Pawley fit (red) of powder X-ray diffraction pattern (λ = 1.5418 Å) for UU-100(Co) against the experimental PXRD pattern (black), showing good agreement factor (weighted-profile R factor R_{wp} = 0.0770 and unweighted-profile R factor R_p = 0.0585 after convergence). (B) SEM image of UU-100(Co) with corresponding energy dispersive X-ray spectroscopy elemental maps of Zr Lα, Co Kα, Cl Kα, and O Kα. The scale bar in the EDX maps represents 1 μm. (C) HRTEM image of UU-100(Co) along [110] that shows lattice fringes with d_{001}= 19.1 Å representing the packing of Zr clusters (dark features). (D) Fourier transform of the image showing the 00l reflections. (E) Enlarged HRTEM image of the region marked by a blue square in C; two Zr cluster columns are marked by red circles. (F) N_2 sorption isotherm at 77 K (closed and open circles denote adsorption and desorption, respectively) and (G) DFT pore size distribution of UU-100(Co).

The structural integrity of the cobaloxime linker in UU-100(Co) was confirmed by ^{1}H NMR spectroscopy of digested samples which exhibits peaks at chemical shifts matching those of pristine [Co(dcpgH)(dcpgH$_2$)]Cl$_2$ (Figure S13). It is very likely that the cobaloxime linkers undergo Cl$^-$/solvent ligand-exchange in the axial position during the solvothermal synthesis, and consequently, the cobaloxime units in UU-100(Co) can have a molecular formula of either [Co(dcpgH)-(dcpgH$_2$)]Cl$_2$ or [Co(dcpgH)$_2$](Cl)(solvent). Thermal stability of the MOF was investigated by thermogravimetric analysis (TGA). The initial weight loss below 100 °C is assigned to removal of guest solvent molecules (Figure S14). Subsequent loss at ~250 °C is attributed to the dehydroxylation of the Zr$_6$ nodes. Above 400 °C, loss of the cobaloxime linker is observed that leads to degradation of the framework and the formation of metal oxide.

Activation of UU-100(Co) by solvent removal either under high vacuum or by solvent exchange with acetone affects the crystallinity of the MOF as evidenced by an altered PXRD pattern (Figure S6). The altered material exhibits three sharp reflections at 4.7°, 9.1°, and 18.0°, while several other reflections that are present in the as-synthesized MOF undergo broadening and decrease in intensity, suggesting partial collapse of the structure. Retention of the reflections corresponding to (001), (002), and (004) planes indicates that the long-range order along the c-axis is preserved. The gas sorption data of the activated material exhibits a reversible type II behavior with a saturated N_2 uptake of 285 cm^3 g^{-1}. The calculated Brunauer–Emmett–Teller (BET) surface area of the MOF was 902 ± 15 m^2 g^{-1} (Figures 1F and S15) with a total pore volume of 0.43 cm^3 g^{-1} as determined by the single-point method. Even though this surface area is obtained for the partially collapsed material, it is significantly higher that of a recently reported HER catalyst based on a porphyrin-based MOF on carbon-nanotubes (Hf$_{12}$-CoDBP/CNT).[36] The theoretical surface area of UU-100(Co) based on the model structure is 2867.9 m^2 g^{-1}, substantially larger than that of the material that is obtained after solvent removal. DFT fitting of the N_2 adsorption data showed a pore width distribution in the range of 12–18 Å (Figure 1G), which is broadly consistent with the modeled structure of UU-100(Co) as described above.

Electrochemical Characterization of UU-100(Co)|FTO. UU-100(Co) was synthesized directly on fluorine-doped tin oxide (FTO) to deduce the basic electrochemical properties of the material. For this purpose, a self-assembled monolayer (SAM) of the cobaloxime linker on the FTO substrate was first formed by soaking the FTO electrodes overnight in a 1 mM solution of Co(dcpgH)(dcpgH$_2$)Cl$_2$ in DMF. The SAM coated FTO slides were subsequently heated in a mixture of ZrCl$_4$, cobaloxime linker, DMF, and acetic acid at 80 °C for 5 days. The PXRD pattern of the as-prepared UU-100(Co)|FTO thin film (Figure 3A) is consistent with that of the bulk material and the SEM images (Figures 3B and S17) show identical particle morphology. SEM-EDX (Figure S20) and ICP-OES analyses of the UU-100(Co)|FTO film reveal Zr:Co ratios of 2.7 ± 0.1 and 3.1 ± 0.2, respectively, consistent with the calculated structure. The film thickness was estimated to be

DOI: 10.1021/jacs.9b07084
J. Am. Chem. Soc. 2019, 141, 15942–15950

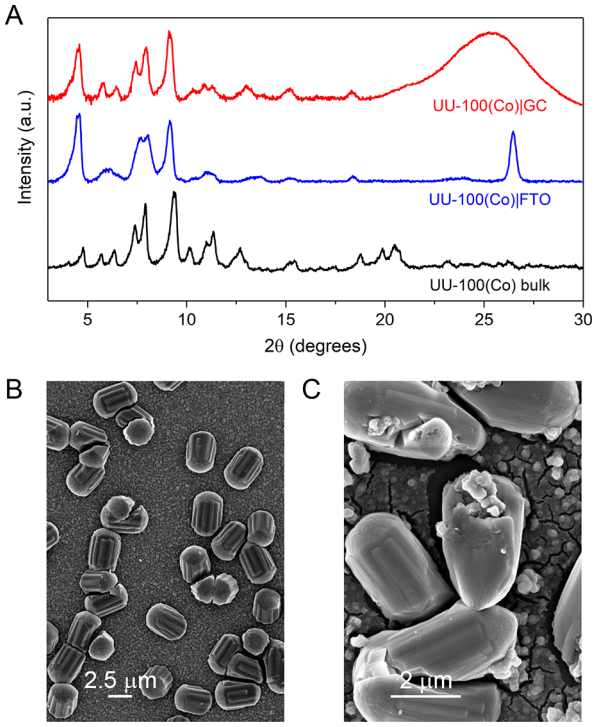

Figure 3. (A) PXRD of UU-100(Co) thin films (λ = 1.5418 Å). SEM images of (B) UU-100(Co)|FTO and (C) UU-100(Co)|GC. Panel (B) shows the rod-shaped UU-100(Co) crystals on a bare FTO surface, while the glassy carbon surface in (C) is coated with the smaller particles of UU-100(Co).

~1 μm from the images obtained by cross-sectional SEM (Figure S18). Similar to the case of bulk UU-100(Co), DMF removal by overnight soaking of the thin-film electrodes in acetone leads to the altered PXRD pattern (Figure S23).

The cobaloxime SAM-modified electrode (SAM|FTO) and UU-100(Co)|FTO were further characterized by X-ray photoelectron spectroscopy (XPS). The SAM of the cobaloxime linker on FTO was confirmed by the Co 2p and N 1s peaks (Figures S21 and S22). The spectra of UU-100(Co)|FTO exhibit four additional zirconium peaks, two at 332.5 and 346.5 corresponding to Zr $3p_{3/2}$ and $3p_{1/2}$, and two more at 181.5 and 183.8 for Zr $3d_{5/2}$ and $3d_{3/2}$, respectively. Two sets of peaks are observed in the cobalt region of UU-100(Co)|FTO, with binding energies of ~781 and ~795 eV, which correspond to the $2p_{3/2}$ and $2p_{1/2}$ levels in the expected 2:1 ratio.[48] Absence of peaks below 779 eV excludes the presence of metallic cobalt on the surface. Deconvolution of the C 1s region generates three peaks at 283.8, 285.2, and 287.6 eV that are attributed to C═C/C−C, C═N, and C═O bonds, respectively (Figure S22).

The cyclic voltammogram (CV) of UU-100(Co)|FTO shows a reversible redox wave with an $E_{1/2}$ = −1.28 V ($E_{p,c}$ = −1.40 V; $E_{p,a}$ = −1.16 V; ν = 0.1 V s^{-1}) that is assigned to the $Co^{II/I}$ couple (Figure 4A). The potential of the $Co^{II/I}$ couple in UU-100(Co)|FTO is shifted cathodically by ~150 mV relative to that of the $Co^{II/I}$ couple in the free cobaloxime reference (Figure S24, see the Supporting Information for details), consistent with the greater negative charge of the tetra-deprotonated linker in the MOF. Reductive features associated with the $Co^{III/II}$ couple are poorly defined in the first CV scan of UU-100(Co)|FTO and completely absent in all subsequent scans. This behavior stems most likely from the partial exchange of the axial chloride ligands with solvent molecules during the solvothermal synthesis, giving rise to mixtures of cobaloxime linkers that differ in the axial ligands. Upon reduction of the cobaloximes from Co^{III} to Co^{I} in the first reductive scan, axial ligands are completely displaced by solvent molecules which pushes the $Co^{III/II}$ couple outside the scanned potential window (Figure S26, see the Supporting Information for details). As a result, all subsequent CV scans of UU-100(Co)|FTO show exclusively the $Co^{II/I}$ couple (Figure 4A).

The amount of electroactive cobaloxime linkers was determined by chronoamperometry. Potential stepping from −0.05 to −1.5 V and from −1.5 to −0.05 V revealed surface concentrations of 7.0×10^{-8} and 6.8×10^{-8} mol cm^{-2} (Figures S27 and S28), respectively. Compared to the total cobalt content of 12.2×10^{-8} mol cm^{-2} as determined by ICP-OES, 54 ± 15% (average over three electrodes) of the cobaloxime linkers in the MOF are electrochemically addressable, which compares favorably to the 31.9% electroactive catalyst centers in a recently reported porphyrin-based MOF on carbon nanotubes.[36]

Exploiting the electrochromism of molecular cobaloximes,[49] UV−vis spectroelectrochemistry can be used to probe the kinetics of electron transport within the film. Under an applied potential of −1.50 V in DMF (0.1 M $LiClO_4$), freshly prepared UU-100(Co)|FTO electrodes undergo a color change from pale yellow to blue with the appearance of new absorption bands at ~520 and 670 nm that arise from $[Co^{I}(dcpgH)_2]$ (Figure 4B and E). Reoxidation of the film by stepping the potential back to −0.05 V results in a color change from blue to red. The color change is accompanied by a bleach of the 670 nm band and a slight red-shift (~1−2 nm) of the 520 nm peak in the UV−vis spectrum. This behavior indicates the formation of $[Co^{II}(dcpgH)_2]$ linkers in the MOF film at −0.05 V and is consistent with the CV results described above in that the $Co^{III/II}$ couple is at a more positive potential once the film has been reduced and the chloride ligands have detached from the cobaloximes. The Co centers in UU-100(Co)|FTO can reversibly be cycled between Co^{II} and Co^{I} as shown by repetitive electrochromic switching experiments, monitoring the absorbance changes at 520 and 670 nm (Figure 4C). After 10 such cycles, PXRD, XPS, and SEM/EDX (Figures 4D, S19, and S23) indicate that the structural integrity of the MOF films is maintained. All spectral assignments are corroborated by the analogous experiments on the homogeneous cobaloxime linker (Figure S32).

Utilizing the diagnostic absorbance of the reduced Co^{I} linker at 670 nm, the concentration of reduced species inside UU-100(Co)|FTO can be directly measured as a function of time. The obtained trace can be used to extract charge transport kinetics by applying the modified Cottrell equation,[24]

$$\Delta A = \frac{2A_{max}\sqrt{D_{app}}}{d_f\sqrt{\pi}}t^{1/2}$$

where A_{max} denotes the absorbance maximum, t is time in seconds, ΔA is the change in absorbance at 670 nm, and d_f is the thickness of the film. A fit of the data yields an apparent diffusion coefficient (D_{app}) of 4.1(±0.8) × 10^{-8} cm^2 s^{-1} (Figure S34) which is several orders of magnitude higher than that of other MOF thin film electrodes with redox-active linkers measured in organic solvents (10^{-11}−10^{-13} cm^2 s^{-1}).[25,30−32]

DOI: 10.1021/jacs.9b07084
J. Am. Chem. Soc. 2019, 141, 15942−15950

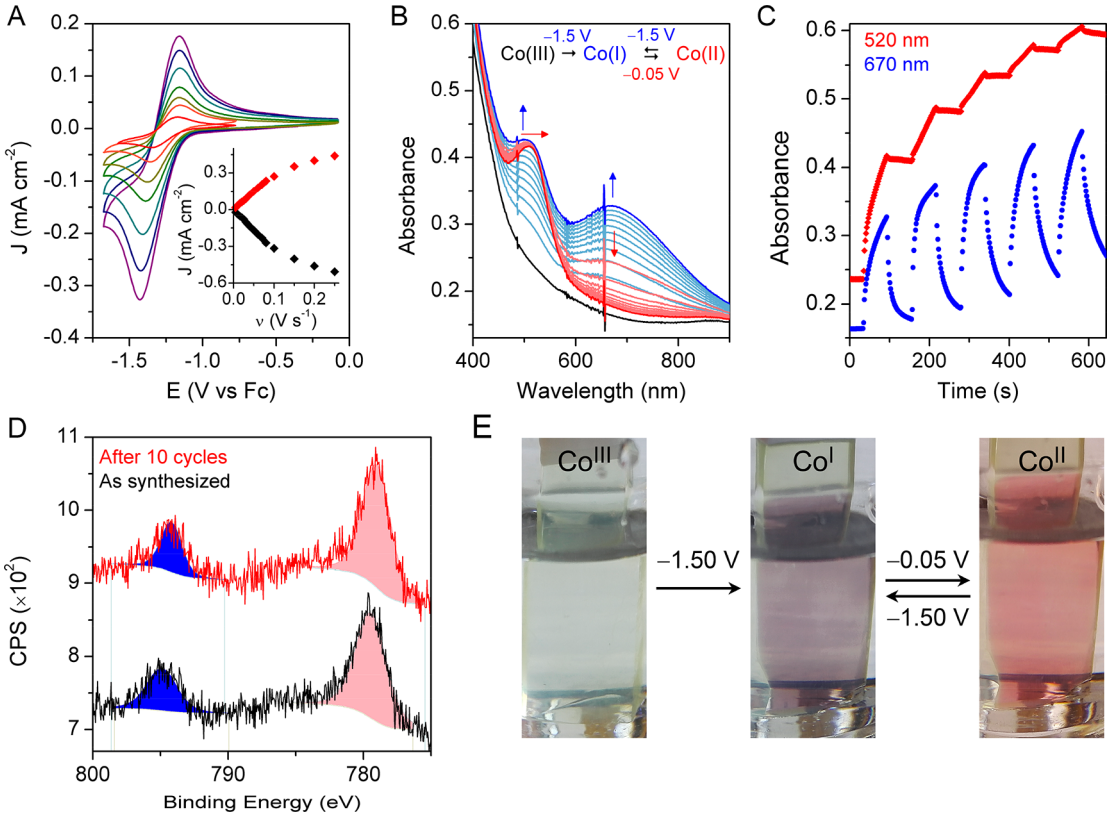

Figure 4. (A) Cyclic voltammograms of UU-100(Co)|FTO electrodes at different scan rates in DMF containing 0.1 M $LiClO_4$ (10, 20, 30, 40, 60, 80, and 100 mV s^{-1}); inset shows the linear dependency of the peak current (Co^{II}/Co^{I} couple) on the scan rate (ν) at scan rates under 100 mV s^{-1}. (B) UV−vis spectroelectrochemical data on UU-100(Co)|FTO thin-film electrodes, showing the steady-state relative absorbance at different applied potentials. (C) Optical transmittance kinetic curve of the UU-100(Co) thin-films measured at 520 and 670 nm by switching the potential from −0.05 to −1.5 V (electrode held at the potential for 60 s). (D) XPS core-level spectra of UU-100(Co)|FTO films showing Co 2p region before (black) and after (red) electrochromic switching tests. Blue and purple filled peaks represent the peak fits corresponding to Co $2p_{1/2}$ and $2p_{3/2}$, respectively. (E) Photographs of the UU-100(Co)|FTO thin films at −0.05 and −1.5 V (vs $Fc^{+/0}$).

Since charge transport in UU-100(Co) films occurs through redox hopping between the redox-active cobaloxime linkers, CVs were recorded at different scan rates to probe the kinetics of the redox process (Figures S29−S31). At slow scan rates (ν = 5−80 mV/s), the cathodic and anodic peak currents of the $Co^{II/I}$ couple show a linear dependence on the scan rate, which is consistent with a surface confined process that is not limited by mass transport (Figure S30). At faster scan rates (>100 mV s^{-1}), however, the peak currents clearly deviate from linear correlation (inset in Figure 4A) and show characteristics of a diffusion-controlled process, as shown by their linear dependence on $\nu^{1/2}$ (Figure S30). This assignment is further corroborated by a double-logarithmic analysis of the voltammetry data which shows that the linear fit of $\log(i_p)$ versus $\log(\nu)$ plot in the slower scan rate region (<80 mV s^{-1}) has a slope of 0.92, whereas the corresponding slope in the faster scan rate range is 0.51 (Figure S31). Such a switch in scan rate dependence has previously been observed by Morris et al. on UiO-67 materials with varying degrees of incorporated redox-active $[Ru(bpy)_3]^{2+}$ linkers[48] but, to the best of our knowledge, has not been observed in one and the same MOF simply by altering the scan rates. Such a behavior is predicted by theory, though, and is well established in the redox polymer film literature.[50] The threshold scan rate at which the peak current responses change from that of a surface-confined to a diffusional process can be calculated from the diffusion coefficient D_{app} and the film thickness d_f according to

$$\frac{1}{d_f}\sqrt{D_{app}\frac{RT}{F\nu}} \approx 1$$

Using the values for UU-100(Co)|FTO determined above, the switching scan rate is calculated to be 100(±25) mV s^{-1} which is in excellent agreement with the experimental value. This observation in a MOF with a significantly high fraction of electrochemically accessible metallo-linkers (>50%) is for the first time enabled by the unmatched high D_{app} in UU-100(Co)|FTO. Related MOF films with redox-active linkers (Co/Fe-porphyrins and naphthalene-diimide) with smaller D_{app} exhibit diffusion-controlled redox processes even at slow scan rates.[24−26,30,32,34]

Electrocatalytic HER by UU-100(Co)|GC. As FTO is unstable in aqueous solution at applied negative potential, UU-100(Co) was grown on glassy carbon (GC) electrodes to study its HER activity. The UU-100(Co)|GC electrodes were prepared under solvothermal conditions on GC that had been functionalized with carboxylic acids by electrochemical diazonium grafting. PXRD and SEM of the UU-100(Co)|GC electrodes were identical to those of the bulk material, confirming its successful formation (Figurse 3 and S35). The concentration of the electroactive cobaloxime linker determined from cyclic voltammetry was ∼1.6 × 10^{-8} mol cm^{-2} which shows the electrochemical accessibility of cobalt centers in GC (31%) is somewhat lower than that observed in the FTO films (Figure 5A). The catalytic performance of UU-

DOI: 10.1021/jacs.9b07084
J. Am. Chem. Soc. 2019, 141, 15942−15950

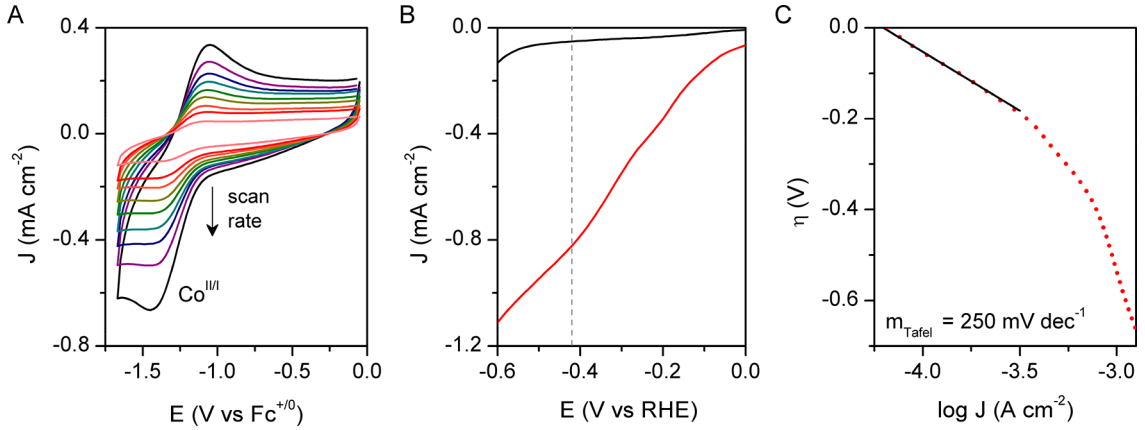

Figure 5. (A) Cyclic voltammograms of UU-100(Co)|GC at different scan rates (0.2, 0.16, 0.14, 0.12, 0.1, 0.8, 0.06, 0.05, and 0.025 V s^{-1}) in DMF. (B) Linear sweep voltammograms of UU-100(Co)|GC (red) and blank GC (black) electrodes at pH 4 recorded at 20 mV s^{-1} (dashed line shows the potential applied for electrolyses experiments). (C) Tafel plot derived from the LSV; black line shows the linear fit of the data in the low-overpotential region.

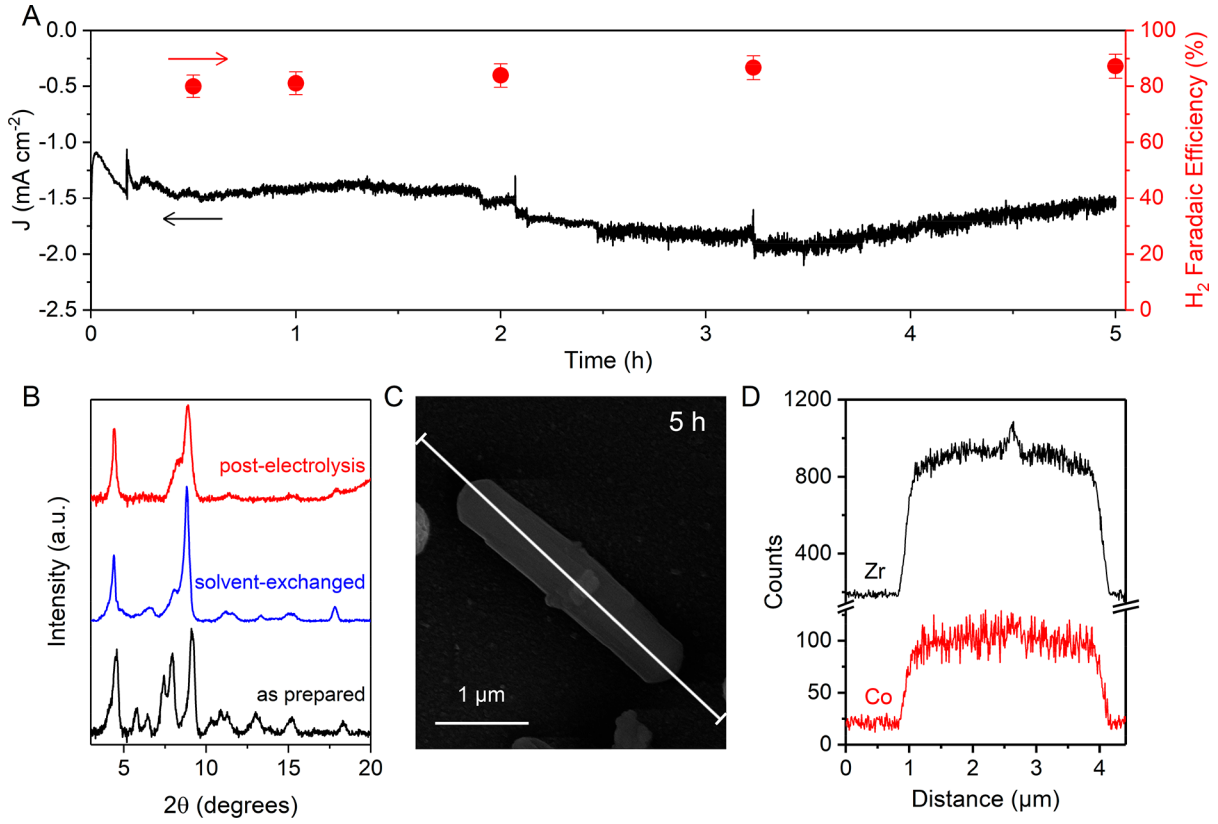

Figure 6. (A) Controlled potential electrolysis using UU-100(Co)|GC electrode at −0.45 V vs RHE in acetate buffer at pH 4. The black trace represents geometric current density, and the red circles denote faradaic efficiency for H_2 evolution. (B) PXRD patterns of the as-synthesized electrodes (black), after solvent exchange with acetone for 24 h (blue), and after 5 h of electrocatalysis (red) demonstrate that the MOF retains its crystalline structure after electrolysis (see Figures S6 and S7 for PXRD of solvent exchanged UU-100(Co)). (C) SEM images of the UU-100(Co)|GC after electrolysis and (D) corresponding EDX line scan showing retention of rodlike morphology and uniform distribution of Zr and Co in the MOF crystal.

100(Co)|GC electrodes was determined by linear sweep voltammetry (LSV) experiments in acetate buffer at pH 4, which showed the evolution of a catalytic wave with an early onset potential of ∼−0.15 V vs RHE (Figure 5B). Tafel analysis of the LSV data gave a Tafel slope of 250 mV dec^{-1} and an exchange current density of $\sim 10^{-4.2}$ A cm^{-2} (Figure 5C).

Controlled potential electrolysis of UU-100(Co)|GC electrodes in $NaClO_4$ (0.1 M)/acetate (0.2 M) buffer at pH 4 and at an applied potential of −0.45 V vs RHE consumes 29 C cm^{-2} charge over 5 h (Figure 6A) with a stable current density of ∼− 1.7 mA cm^{-2}. Analysis of the gas mixture in the headspace of the working compartment of the electrolysis cell by gas chromatography confirmed evolution of 66 μmol H_2 (geometric surface area of electrode = 0.5 cm^2) with a faradaic

DOI: 10.1021/jacs.9b07084
J. Am. Chem. Soc. 2019, 141, 15942−15950

yield of 84 ± 5%. This corresponds to a turnover number (TON_{Co}) of 8250 based on the amount of electroactive cobalt in the film, with an average formal turnover frequency (TOF_{Co}) of 1650 h^{-1}. Unmodified GC electrodes display much lower H_2-evolution activity under the same conditions (Figure S44). The MOF films show high durability as demonstrated by their sustained activity over the course of 18 h of electrolysis at pH 4 (Figure S37) during which 309 μmol H_2 cm^{-2} was generated with 79 ± 3% faradaic efficiency (FE_{H_2}). A total TON_{Co} of 20 875 was obtained after 18 h along with an average TOF_{Co} of 1171 h^{-1}. The relatively lower TON_{Co} value obtained from long-term electrolysis is likely caused by H_2 leakage leading to low FE_{H_2}. Postcatalysis structural integrity of the framework was probed by PXRD analysis of UU-100(Co)|GC electrodes which shows that the two major reflections at ~4.5° and ~9° were present even after 18 h electrolysis (Figures 6B and S38). This is consistent with the presence of the partially collapsed structure that is also obtained by DMF solvent removal from the as-prepared UU-100(Co) without any applied bias. SEM-EDX analysis of the MOF film after electrolysis showed the largely unchanged rodlike morphology. Additionally, the elemental composition of UU-100(Co) remained intact as demonstrated by the EDX line profile of the MOF particles on the electrode (Figures S39–S43) and a similar Zr:Co ratio of 2.4 ± 0.2 (Figures 6 and S43). However, prolonged electrolysis (18 h) damages the smooth exterior of the crystals significantly and causes flaking of the MOF nanosheets, leading to a rough surface as shown by SEM image (Figure S44).

The cobaloxime linkers are coordination compounds, and as the crystallinity and morphology of UU-100(Co) is preserved during electrolysis, the linkers must have remained intact. With structurally uncompromised HECs, there is no reason to suspect that catalysis is not molecular in nature. The performance of UU-100(Co)|GC as a HEC is vastly superior to that of the most efficient electrocatalytic materials with analogous molecular cobaloxime catalysts. Such systems have been immobilized on carbon nanotubes (CNTs) and CNT–polymer composites and are reported to support 120 and 420 turnovers, respectively, at near neutral pH.[51,52] The molecular cobaloxime linker itself displayed a TON of 10 under homogeneous conditions, 2 h of electrolysis in mildly acidic aqueous solution (Figure S46). These TONs are substantially lower than the TON_{Co} observed for UU-100(Co) (more than 20 000) which highlights the stabilization of the cobaloxime core provided by the rigid 3D architecture of the framework. In comparison to the only other electrocatalytic MOF for hydrogen evolution, (Hf_{12}-CoDBP/CNT), UU-100(Co) displays a slower rate but operates under milder conditions (pH 4 versus pH 0) and without any Nafion binder to maintain stable current densities.[36] From a more fundamental perspective, an important distinction between the two electrocatalytic MOFs is the necessity of growing the MOF on carboxylated CNTs for realizing the HER activity in the case of Hf_{12}-CoDPB, which emphasizes the excellent "molecular-wiring" in UU-100(Co) imparted by the cobaloxime linkers.

CONCLUSION

The present work describes electrocatalytic hydrogen evolution by a MOF that exclusively consists of molecular HECs, specifically cobaloximes, as metallo-linkers. Structure elucidation by cRED reveals that UU-100(Co) contains rectangular channels with elliptical pores. $Zr_6(\mu_3\text{-}O)_8(OH)_8$ clusters constitute the SBUs with 8 of the 12 octahedral edges being connected to the cobaloxime linkers. UU-100(Co) can be grown directly on conducting substrates, which allows for in-depth study of the materials' electrochemical and charge transport properties. The individual cobaloxime units in UU-100(Co) function as both redox mediator and catalyst. The CV response of the films is not limited by diffusion, indicating fast electron transport kinetics which is further corroborated by direct spectroelectrochemical methods on UU-100(Co)|FTO. The apparent diffusion coefficient that takes account of contributions from both electron hopping as well as electrolyte diffusion was determined to be 4.1 (±0.8) × 10^{-8} cm^2 s^{-1}, which is orders of magnitude higher than that of related porphyrin-based MOF thin films.[30−33] The structural integrity of the molecular cobaloxime catalyst is greatly enhanced by MOF incorporation, and consequently, electrocatalytic hydrogen evolution from water at pH = 4 by UU-100(Co)|GC is highly durable for at least 18 h.

This paper is a proof-of-concept study that illustrates that structurally fragile molecular catalysts can be stabilized by MOF incorporation so that they can be used as electrocatalysts for extended periods of time. More specifically, the structural integrity of the cobaloximes is greatly improved, and as a result the obtained TONs are orders of magnitude (at least 50–200 times) higher than those of any other related system that utilize similar cobaloxime HECs. The high porosity and large internal channels in UU-100(Co) allow easy catalyst access, and the spatial proximity of the redox-active metallo-linkers promotes high electron hopping rates. The present study will inspire future works using similar concepts, potentially paired with refined film thickness control or chemical alterations at, or close to, the catalyst. More specifically, for UU-100(Co), these may include the coordination of pyridine ligands to the cobaloximes or of proton shuttling groups to the free coordination sites of the SBUs.[38] Such developments will further close the gap between molecular and materials catalysis, potentially even by including higher coordination sphere active site concepts from bioinorganic chemistry.

ASSOCIATED CONTENT

Supporting Information

The Supporting Information is available free of charge on the ACS Publications website at DOI: 10.1021/jacs.9b07084.

General methods and instrumentation, synthetic details, characterization of materials, electrode fabrication, and additional electrochemical data (PDF)

Crystallographic data for the cobaloxime metallolinker (CIF)

AUTHOR INFORMATION

Corresponding Author

*sascha.ott@kemi.uu.se

ORCID

Souvik Roy: 0000-0003-0146-5283

Xiaodong Zou: 0000-0001-6748-6656

Sascha Ott: 0000-0002-1691-729X

Author Contributions

§S.R. and Z.H. contributed equally.

Notes

The authors declare no competing financial interest.

DOI: 10.1021/jacs.9b07084
J. Am. Chem. Soc. 2019, 141, 15942−15950

Crystallographic data for the cobaloxime metallolinker has been deposited at the Cambridge Crystallographic Data Centre under deposition no. CCDC 1910684.

■ ACKNOWLEDGMENTS

Financial support from the Wenner-Gren Foundations (postdoctoral stipend to S.R.), the European Research Council (ERC-CoG2015-681895_MOFcat), the Swedish Research Council, and the Swedish Energy Agency is gratefully acknowledged. Z.H. and X.Z. acknowledge the support by the CATSS project (2016.0072) from the Knut and Alice Wallenberg Foundation (KAW) and the Swedish Research Council (VR, 2017-04321). Dr. Jean Pettersson is acknowledged for ICP-OES measurements. Mr. Ben Johnson and Dr. Brian McCarthy are acknowledged for valuable discussions.

■ REFERENCES

(1) Ogden, J. M. Prospects for Building a Hydrogen Energy Infrastructure. *Annu. Rev. Energy Env.* **1999**, *24*, 227.
(2) Edwards, P. P.; Kuznetsov, V. L.; David, W. I. F.; Brandon, N. P. Hydrogen and fuel cells: Towards a sustainable energy future. *Energy Policy* **2008**, *36*, 4356.
(3) Turner, J. A. Sustainable Hydrogen Production. *Science* **2004**, *305*, 972.
(4) Vesborg, P. C. K.; Seger, B.; Chorkendorff, I. Recent Development in Hydrogen Evolution Reaction Catalysts and Their Practical Implementation. *J. Phys. Chem. Lett.* **2015**, *6*, 951.
(5) Zeng, M.; Li, Y. Recent Advances in Heterogeneous Electrocatalysts for the Hydrogen Evolution Reaction. *J. Mater. Chem. A* **2015**, *3*, 14942.
(6) Gray, H. B. Powering the Planet with Solar Fuel. *Nat. Chem.* **2009**, *1*, 7.
(7) Yin, H.; Zhao, S.; Zhao, K.; Muqsit, A.; Tang, H.; Chang, L.; Zhao, H.; Gao, Y.; Tang, Z. Ultrathin Platinum Nanowires Grown on Single-Layered Nickel Hydroxide with High Hydrogen Evolution Activity. *Nat. Commun.* **2015**, *6*, 6430.
(8) Esposito, D. V.; Hunt, S. T.; Stottlemyer, A. L.; Dobson, K. D.; McCandless, B. E.; Birkmire, R. W.; Chen, J. G. Low-Cost Hydrogen-Evolution Catalysts Based on Monolayer Platinum on Tungsten Monocarbide Substrates. *Angew. Chem., Int. Ed.* **2010**, *49*, 9859.
(9) Cheng, N.; Stambula, S.; Wang, D.; Banis, M. N.; Liu, J.; Riese, A.; Xiao, B.; Li, R.; Sham, T.-K.; Liu, L.-M.; Botton, G. A.; Sun, X. Platinum Single-Atom and Cluster Catalysis of the Hydrogen Evolution Reaction. *Nat. Commun.* **2016**, *7*, 13638.
(10) Konkena, B.; junge Puring, K.; Sinev, I.; Piontek, S.; Khavryuchenko, O.; Dürholt, J. P.; Schmid, R.; Tüysüz, H.; Muhler, M.; Schuhmann, W.; Apfel, U.-P. Pentlandite Rocks as Sustainable and Stable Efficient Electrocatalysts for Hydrogen Generation. *Nat. Commun.* **2016**, *7*, 12269.
(11) Tran, P. D.; Tran, T. V.; Orio, M.; Torelli, S.; Truong, Q. D.; Nayuki, K.; Sasaki, Y.; Chiam, S. Y.; Yi, R.; Honma, I.; Barber, J.; Artero, V. Coordination Polymer Structure and Revisited Hydrogen Evolution Catalytic Mechanism for Amorphous Molybdenum Sulfide. *Nat. Mater.* **2016**, *15*, 640.
(12) Roger, I.; Shipman, M. A.; Symes, M. D. Earth-Abundant Catalysts for Electrochemical and Photoelectrochemical Water Splitting. *Nat. Rev. Chem.* **2017**, *1*, No. 0003.
(13) Voiry, D.; Yamaguchi, H.; Li, J.; Silva, R.; Alves, D. C. B.; Fujita, T.; Chen, M.; Asefa, T.; Shenoy, V. B.; Eda, G.; Chhowalla, M. Enhanced catalytic activity in strained chemically exfoliated WS2 nanosheets for hydrogen evolution. *Nat. Mater.* **2013**, *12*, 850.
(14) Dalle, K. E.; Warnan, J.; Leung, J. J.; Reuillard, B.; Karmel, I. S.; Reisner, E. Electro- and Solar-Driven Fuel Synthesis with First Row Transition Metal Complexes. *Chem. Rev.* **2019**, *119*, 2752.
(15) Liu, J.; Chen, L.; Cui, H.; Zhang, J.; Zhang, L.; Su, C.-Y. Applications of metal−organic frameworks in heterogeneous supramolecular catalysis. *Chem. Soc. Rev.* **2014**, *43*, 6011.
(16) Majewski, M. B.; Peters, A. W.; Wasielewski, M. R.; Hupp, J. T.; Farha, O. K. Metal−Organic Frameworks as Platform Materials for Solar Fuels Catalysis. *ACS Energy Lett.* **2018**, *3*, 598.
(17) Stassen, I.; Burtch, N.; Talin, A.; Falcaro, P.; Allendorf, M.; Ameloot, R. An updated roadmap for the integration of metal−organic frameworks with electronic devices and chemical sensors. *Chem. Soc. Rev.* **2017**, *46*, 3185.
(18) Mijangos, E.; Roy, S.; Pullen, S.; Lomoth, R.; Ott, S. Evaluation of two- and three-dimensional electrode platforms for the electrochemical characterization of organometallic catalysts incorporated in non-conducting metal−organic frameworks. *Dalton Trans.* **2017**, *46*, 4907.
(19) Johnson, B. A.; Bhunia, A.; Ott, S. Electrocatalytic water oxidation by a molecular catalyst incorporated into a metal−organic framework thin film. *Dalton Trans.* **2017**, *46*, 1382.
(20) Wang, T. C.; Hod, I.; Audu, C. O.; Vermeulen, N. A.; Nguyen, S. T.; Farha, O. K.; Hupp, J. T. Rendering High Surface Area, Mesoporous Metal−Organic Frameworks Electronically Conductive. *ACS Appl. Mater. Interfaces* **2017**, *9*, 12584.
(21) Zhao, S.; Wang, Y.; Dong, J.; He, C.-T.; Yin, H.; An, P.; Zhao, K.; Zhang, X.; Gao, C.; Zhang, L.; Lv, J.; Wang, J.; Zhang, J.; Khattak, A. M.; Khan, N. A.; Wei, Z.; Zhang, J.; Liu, S.; Zhao, H.; Tang, Z. Ultrathin metal−organic framework nanosheets for electrocatalytic oxygen evolution. *Nat. Energy* **2016**, *1*, 16184.
(22) Duan, J.; Chen, S.; Zhao, C. Ultrathin metal-organic framework array for efficient electrocatalytic water splitting. *Nat. Commun.* **2017**, *8*, 15341.
(23) Sun, L.; Campbell, M. G.; Dincă, M. Electrically Conductive Porous Metal−Organic Frameworks. *Angew. Chem., Int. Ed.* **2016**, *55*, 3566.
(24) Ahrenholtz, S. R.; Epley, C. C.; Morris, A. J. Solvothermal Preparation of an Electrocatalytic Metalloporphyrin MOF Thin Film and its Redox Hopping Charge-Transfer Mechanism. *J. Am. Chem. Soc.* **2014**, *136*, 2464.
(25) Johnson, B. A.; Bhunia, A.; Fei, H.; Cohen, S. M.; Ott, S. Development of a UiO-Type Thin Film Electrocatalysis Platform with Redox-Active Linkers. *J. Am. Chem. Soc.* **2018**, *140*, 2985.
(26) Wade, C. R.; Li, M.; Dincă, M. Facile Deposition of Multicolored Electrochromic Metal−Organic Framework Thin Films. *Angew. Chem., Int. Ed.* **2013**, *52*, 13377.
(27) Kung, C.-W.; Wang, T. C.; Mondloch, J. E.; Fairen-Jimenez, D.; Gardner, D. M.; Bury, W.; Klingsporn, J. M.; Barnes, J. C.; Van Duyne, R.; Stoddart, J. F.; Wasielewski, M. R.; Farha, O. K.; Hupp, J. T. Metal−Organic Framework Thin Films Composed of Free-Standing Acicular Nanorods Exhibiting Reversible Electrochromism. *Chem. Mater.* **2013**, *25*, 5012.
(28) AlKaabi, K.; Wade, C. R.; Dincă, M. Transparent-to-Dark Electrochromic Behavior in Naphthalene-Diimide-Based Mesoporous MOF-74 Analogs. *Chem.* **2016**, *1*, 264.
(29) Downes, C. A.; Marinescu, S. C. Electrocatalytic Metal−Organic Frameworks for Energy Applications. *ChemSusChem* **2017**, *10*, 4374.
(30) Hod, I.; Sampson, M. D.; Deria, P.; Kubiak, C. P.; Farha, O. K.; Hupp, J. T. Fe-Porphyrin-Based Metal−Organic Framework Films as High-Surface Concentration, Heterogeneous Catalysts for Electrochemical Reduction of CO_2. *ACS Catal.* **2015**, *5*, 6302.
(31) Lin, S.; Diercks, C. S.; Zhang, Y.-B.; Kornienko, N.; Nichols, E. M.; Zhao, Y.; Paris, A. R.; Kim, D.; Yang, P.; Yaghi, O. M.; Chang, C. J. Covalent organic frameworks comprising cobalt porphyrins for catalytic CO_2 reduction in water. *Science* **2015**, *349*, 1208.
(32) Kornienko, N.; Zhao, Y.; Kley, C. S.; Zhu, C.; Kim, D.; Lin, S.; Chang, C. J.; Yaghi, O. M.; Yang, P. Metal−Organic Frameworks for Electrocatalytic Reduction of Carbon Dioxide. *J. Am. Chem. Soc.* **2015**, *137*, 14129.
(33) Dong, B.-X.; Qian, S.-L.; Bu, F.-Y.; Wu, Y.-C.; Feng, L.-G.; Teng, Y.-L.; Liu, W.-L.; Li, Z.-W. Electrochemical Reduction of CO2 to CO by a Heterogeneous Catalyst of Fe−Porphyrin-Based Metal−Organic Framework. *ACS Appl. Energy Mater.* **2018**, *1*, 4662.

DOI: 10.1021/jacs.9b07084
J. Am. Chem. Soc. 2019, 141, 15942−15950

(34) Usov, P. M.; Huffman, B.; Epley, C. C.; Kessinger, M. C.; Zhu, J.; Maza, W. A.; Morris, A. J. Study of Electrocatalytic Properties of Metal−Organic Framework PCN-223 for the Oxygen Reduction Reaction. *ACS Appl. Mater. Interfaces* **2017**, *9*, 33539.
(35) Su, C.-H.; Kung, C.-W.; Chang, T.-H.; Lu, H.-C.; Ho, K.-C.; Liao, Y.-C. Inkjet-Printed Porphyrinic Metal−Organic Framework Thin Films for Electrocatalysis. *J. Mater. Chem. A* **2016**, *4*, 11094.
(36) Micheroni, D.; Lan, G.; Lin, W. Efficient Electrocatalytic Proton Reduction with Carbon Nanotube-Supported Metal−Organic Frameworks. *J. Am. Chem. Soc.* **2018**, *140*, 15591.
(37) Dong, R.; Pfeffermann, M.; Liang, H.; Zheng, Z.; Zhu, X.; Zhang, J.; Feng, X. Large-Area, Free-Standing, Two-Dimensional Supramolecular Polymer Single-Layer Sheets for Highly Efficient Electrocatalytic Hydrogen Evolution. *Angew. Chem., Int. Ed.* **2015**, *54*, 12058.
(38) Clough, A. J.; Yoo, J. W.; Mecklenburg, M. H.; Marinescu, S. C. Two-Dimensional Metal−Organic Surfaces for Efficient Hydrogen Evolution from Water. *J. Am. Chem. Soc.* **2015**, *137*, 118.
(39) Downes, C. A.; Marinescu, S. C. Efficient Electrochemical and Photoelectrochemical H2 Production from Water by a Cobalt Dithiolene One-Dimensional Metal−Organic Surface. *J. Am. Chem. Soc.* **2015**, *137*, 13740.
(40) Dong, R.; Zheng, Z.; Tranca, D. C.; Zhang, J.; Chandrasekhar, N.; Liu, S.; Zhuang, X.; Seifert, G.; Feng, X. Immobilizing Molecular Metal Dithiolene−Diamine Complexes on 2D Metal−Organic Frameworks for Electrocatalytic H2 Production. *Chem. - Eur. J.* **2017**, *23*, 2255.
(41) Noh, H.; Kung, C.-W.; Otake, K.-i.; Peters, A. W.; Li, Z.; Liao, Y.; Gong, X.; Farha, O. K.; Hupp, J. T. Redox-Mediator-Assisted Electrocatalytic Hydrogen Evolution from Water by a Molybdenum Sulfide-Functionalized Metal−Organic Framework. *ACS Catal.* **2018**, *8*, 9848.
(42) Hod, I.; Deria, P.; Bury, W.; Mondloch, J. E.; Kung, C.-W.; So, M.; Sampson, M. D.; Peters, A. W.; Kubiak, C. P.; Farha, O. K.; Hupp, J. T. A Porous Proton-Relaying Metal-Organic Framework Material that Accelerates Electrochemical Hydrogen Evolution. *Nat. Commun.* **2015**, *6*, 8304.
(43) Warren, M. 'Why didn't we think to do this earlier?' Chemists Thrilled by Speedy Atomic Structures. *Nature* **2018**, *563*, 16.
(44) Wan, W.; Sun, J.; Su, J.; Hovmoller, S.; Zou, X. Three-dimensional rotation electron diffraction: software RED for automated data collection and data processing. *J. Appl. Crystallogr.* **2013**, *46*, 1863.
(45) Dempsey, J. L.; Brunschwig, B. S.; Winkler, J. R.; Gray, H. B. Hydrogen Evolution Catalyzed by Cobaloximes. *Acc. Chem. Res.* **2009**, *42*, 1995.
(46) Guillerm, V.; Gross, S.; Serre, C.; Devic, T.; Bauer, M.; Ferey, G. A zirconium methacrylate oxocluster as precursor for the low-temperature synthesis of porous zirconium(iv) dicarboxylates. *Chem. Commun.* **2010**, *46*, 767.
(47) Serre, C.; Millange, F.; Surblé, S.; Férey, G. A Route to the Synthesis of Trivalent Transition-Metal Porous Carboxylates with Trimeric Secondary Building Units. *Angew. Chem., Int. Ed.* **2004**, *43*, 6285.
(48) Chuang, T. J.; Brundle, C. R.; Rice, D. W. Interpretation of the x-ray photoemission spectra of cobalt oxides and cobalt oxide surfaces. *Surf. Sci.* **1976**, *59*, 413.
(49) Scherer, M. R. J.; Muresan, N. M.; Steiner, U.; Reisner, E. RYB tri-colour electrochromism based on a molecular cobaloxime. *Chem. Commun.* **2013**, *49*, 10453.
(50) Andrieux, C. P.; Savéant, J. M. Electron transfer through redox polymer films. *J. Electroanal. Chem.* **1980**, *111*, 377.
(51) Reuillard, B.; Warnan, J.; Leung, J. J.; Wakerley, D. W.; Reisner, E. A Poly(cobaloxime)/Carbon Nanotube Electrode: Freestanding Buckypaper with Polymer-Enhanced H2-Evolution Performance. *Angew. Chem., Int. Ed.* **2016**, *55*, 3952.
(52) Donck, S.; Fize, J.; Gravel, E.; Doris, E.; Artero, V. Supramolecular assembly of cobaloxime on nanoring-coated carbon nanotubes: addressing the stability of the pyridine−cobalt linkage under hydrogen evolution turnover conditions. *Chem. Commun.* **2016**, *52*, 11783.

DOI: 10.1021/jacs.9b07084
J. Am. Chem. Soc. 2019, 141, 15942−15950